Submitted: 16 September, 2023 Accepted: 26 October, 2023 Published: 08 November, 2023 DOI:10.22514/sv.2023.113

Open Access

Signa Vitae

ORIGINAL RESEARCH

Chac1 silencing mitigates hemorrhagic shock-induced intestinal injury by inhibiting oxidative stress and ferroptosis

Hao Yao[1,†], Yan Wang[1,†], Wuming Zhou[1], Ce Xu[1], Xin Ge[1,2,*], Jiandong Zhu[3,*]

[1]Department of Critical Care Medicine, Wuxi 9th People's Hospital Affiliated to Soochow University, 214000 Wuxi, Jiangsu, China
[2]Orthopedic Institution of Wuxi City, 214000 Wuxi, Jiangsu, China
[3]Department of Gastroenterology, Wuxi 9th People's Hospital Affiliated to Soochow University, 214000 Wuxi, Jiangsu, China

***Correspondence**
zjd184@163.com
(Jiandong Zhu);
gexin2021@suda.edu.cn
(Xin Ge)

† These authors contributed equally.

Abstract

Hemorrhagic shock (HS) is a common and significant cause of mortality and morbidity, often resulting in structural damage and dysfunction of the intestines. ChaC glutathione-specific gamma-glutamylcyclotransferase 1 (Chac1) has been reported to be involved in the regulation of oxidative stress and ferroptosis in mammals. Herein, we investigate the effects of Chac1 on HS-induced intestinal injury induced by HS both *in vitro* and *in vivo*. Sprague-Dawley rat model with HS was established, and our investigations showed upregulation of the mRNA and protein levels of Chac1 in the model's ileum tissues. Histopathological analysis revealed that knockdown of Chac1 attenuated the intestinal injury induced by HS. Depletion of Chac1 also reduced the increase in intestinal fatty acid binding protein (I-FABP) concentration. Immunofluorescence staining indicated that silencing Chac1 significantly suppressed the downregulation of occludin and zonula occludens-1 (ZO-1). HS-induced changes in lipid peroxidation (LPO), malondialdehyde (MDA), and glutathione (GSH) levels were reversed in the absence of Chac1, suggesting that downregulation of Chac1 alleviated HS-induced oxidative stress. Additionally, HS led to a decrease in glutathione peroxidase 4 (Gpx4) and ferritin heavy chain 1 (Fth1) expression, along with an increase in ferrous ion (Fe^{2+}) concentration. Knockdown of Chac1 significantly inhibited ferroptosis by increasing Gpx4 and Fth1 expression while reducing the Fe^{2+} concentration. *In vitro* experiments using the rat small intestine crypt epithelial cells (IEC-6) demonstrated that depletion of Chac1 suppressed oxidative stress and ferroptosis induced by hypoxia/reoxygenation (H/R). In conclusion, our study provides evidence that downregulation of Chac1 mitigates HS-induced intestinal injury by inhibiting oxidative stress and ferroptosis.

Keywords

Chac1; Hemorrhagic shock; Intestinal injury; Oxidative stress; Ferroptosis

1. Introduction

Hemorrhagic shock (HS), primarily caused by vascular rupture and extensive tissue damage, is a prevalent cause of mortality and disability worldwide [1, 2]. It induces a critical deficiency in the supply of oxygen and vital nutrients essential for cell survival [3]. Previous studies have reported that HS can initiate multiple organ damage, giving rise to a condition known as multiorgan dysfunction syndrome (MODS), largely due to the induction of cellular hypoxia [4]. The intestine, a crucial organ responsible for maintaining nutrient absorption and toxin excretion homeostasis [5], has been documented to suffer injuries and functional disruptions as a consequence of HS [6]. During HS resuscitation, an imbalanced reduction in intestinal blood flow often results in mucosal barrier injury, exacerbating the compromise of both barrier and absorptive functions [7, 8]. Severe intestinal HS injury is accompanied by alterations of the intestinal flora and the release of bacterial toxins into the bloodstream [9], subsequently triggering systemic inflammation and, in some instances, leading to multiple organ failure [10, 11]. The present effective strategies for preventing HS-induced injuries remain elusive, with limited clinical outcomes to guide intervention [12]. Possibly related to the incompletely understood pathogenesis underlying HS-induced intestinal dysfunction.

In our previous research utilizing high-throughput sequencing of ileum tissue from an HS rat model, we observed a notable increase in the expression of ChaC glutathione-specific gamma-glutamylcyclotransferase 1 (Chac1) within the ileum tissue of these HS rats. Chac1, a constituent of the unfolded protein response (UPR) in mammals [13], is known for its role in promoting apoptosis and involvement in oxidative stress and apoptosis through various signaling pathways and factors [14]. Oxidative stress and ferroptosis are pivotal factors

This is an open access article under the CC BY 4.0 license (https://creativecommons.org/licenses/by/4.0/).
 ©2023 The Author(s). Published by MRE Press.

contributing to organ damage resulting from HS [15, 16]. Specifically, ferroptosis induced by HS is characterized by iron accumulation and a reduction in glutathione peroxidase 4 (Gpx4) levels [17, 18]. In addition, Chac1 has been reported to suppress the expression of glutathione (GSH), whose depletion of GSH triggers ferroptosis of mammalian cells [19, 20]. A recent study demonstrated that reducing Chac1 levels alleviates oxidative stress and ferroptosis by modulating GSH levels and Gpx4 expression [21]. As a component of the UPR pathway, Chac1 plays a role in promoting cell ferroptosis by modulating GSH depletion in retinal pigment epithelial cells [22]. Moreover, Chac1 has been identified as a biomarker with a tumor-suppressive function in renal clear cell carcinoma [23]. However, whether Chac1 influences the intestinal injury by modulating oxidative stress and ferroptosis remains a subject that requires further investigation.

In this present study, we evaluated the expression of Chac1 in a rat model of HS, and following the *in vivo* knockdown of Chac1, the concentration of intestinal fatty acid binding protein (I-FABP) in the model's plasma was measured. In addition, we assessed the expression of occludin and zonula occludens-1 (ZO-1) to elucidate the impact of Chac1 on intestinal injury and observed that the downregulation of Chac1 effectively mitigated oxidative stress and ferroptosis within the ileum tissue of HS rat model.

2. Methods and materials

2.1 Establishment of hemorrhagic shock (HS) model

Male Sprague-Dawley rats, aged 12 weeks, were randomly assigned to the following experimental groups: (1) sham (n = 6), HS (n = 8); (2) sham, HS, HS + lentivirus carried negative control short hairpin RNA (LV-shNC), HS + lentivirus carried short hairpin RNA targeting Chac1 (LV-shChac1). Considering the possibility of animal death in the process of modeling, two rats were used as backup in the model group. All rats were housed under standard conditions with a 12 h light/dark cycles and provided *ad libitum* access to food. The HS-induced rat model was established as previously described [24]. Briefly, we surgically isolated the bilateral femoral arteries and one femoral vein were isolated after dissecting the groin area of the rats after anesthetization. Their mean arterial pressure was continuously monitored through the right femoral artery, while the left femoral artery was cannulated for controlled hemorrhage until maintaining the blood pressure within the range of 35–40 mmHg. Then, after maintaining this hypotensive shock state for 90 min, we restored their blood pressure to normal levels by infusing lactated Ringer's solution (three times the volume of bleeding) *via* the femoral vein catheter. Rats undergoing the same surgical procedure without blood loss were designated as the sham group. Prior to the initiation of the HS model, lentivirus containing either shNC (5′-TTCTCCGAACGTGTCACGT-3′) or shChac1 (5′-GACTTTGCCTACAGCGACAGC-3′) at a concentration of 1×10^9 TU/mL was separately administered *via* the tail vein and were classified as the HS + LV-shNC and HS + LV-shChac1 groups. Subsequently, after a 2-hour recovery period in their cages following removal of the cannula, ligation of the vessel, and sterile sutures, blood samples were collected, and their ileal tissues were harvested for subsequent experiments. The mortality rate of animals during model establishment was approximately 20%.

2.2 Cell culture

Intestinal epithelial cells, namely IEC-6 cells, were purchased from iCell Bioscience (Shanghai, China) and cultured in dulbecco's modified eagle medium (DMEM) (iCell Bioscience, Shanghai, China) containing 10% fetal bovine serum (11011-8611, Tianhang Biotechnology, Huzhou, China) in an incubator with 5% CO_2 at 37 °C. After 48 h of transfection using shNC and shChac1 with Lipofectamine 3000 (L3000015, Invitrogen, Carlsbad, CA, USA), the cells were cultured in an incubator with 1% O_2, 94% N_2 and 5% CO_2 for 4 h, followed by 3 h culturing in conditions of normal oxygen content.

2.3 Hematoxylin and eosin (H&E) staining

The ileum tissue samples embedded in paraffin and sectioned into slices measuring 5 μm in thickness. Then, the paraffin was removed using alcohol, and the ileum sections were stained using hematoxylin (H8070, Solarbio, Beijing, China) and eosin (A600190, Sangon Biotech, Shanghai, China). Subsequently, histopathological images were captured and examined using a BX53 microscope (Olympus, Tokyo, Japan). The extent of ileum injury was then evaluated and graded following the criteria established by Chiu *et al.* [25]: where Grade 0 represents normal intestinal mucosa, Grade 1 indicates subepithelial Gruenhagen's space at the tip of the villi, Grade 2 involves an enlarged subepithelial space with moderate epithelial elevation, Grade 3 includes numerous epithelial elevations, potentially with some villi shedding, Grade 4 signifies villi shedding, lamina propria exposure, and capillaries exposed, and Grade 5 denotes lamina propria collapse, ulceration, and bleeding. The histopathological scoring was conducted in a blinded manner to ensure unbiased assessment.

2.4 Real-time quantitative PCR (RT-qPCR)

Total RNA was extracted from the ileum tissue and IEC-6 cells using TRIpure reagent (RP1001, BioTeke, Beijing, China). Briefly, 1 mL of TRIpure lysate was added to the sample, thoroughly mixed, and left at room temperature for 5 min. Subsequently, 200 μL of chloroform was introduced to the mixture, followed by another 3-min incubation at room temperature. After centrifugation at 10,000 g at 4 °C for 10 min, the lower aqueous phase was transferred to a fresh centrifuge tube. An equal volume of isopropanol was added, and the reaction was allowed to proceed overnight at −20 °C. Following centrifugation at 10,000 g at 4 °C for 10 min, the supernatant was discarded, and 1 mL of 75% ethanol was added. Centrifugation at 3400 g for 3 min at 4 °C was performed, after which the supernatant was removed, and the precipitate was allowed to air-dry for 5 min at room temperature. Finally, the total RNA was dissolved in 30 μL of RNase-free ddH_2O, and the concentration of each sample was determined using a UV spectrophotometer NANO 2000

(Thermo Scientific, Pittsburgh, PA, USA). Subsequently, a reverse-transcriptase reaction was performed using the BeyoRT II M-MLV Reverse Transcriptase Kit (D7160L, Beyotime Biotech, Shanghai, China) and RNase inhibitor (B600478, Sangon Biotech, Shanghai, China). Equal amounts of RNA, 1 μL oligo $(dT)_{15}$ and 1 μL random were added to a nuclease-free centrifuge tube, and ddH_2O was added to reach a total reaction volume to 12.5 μL. Then, the mixture was incubated at 70 °C for 5 min and quickly cooled on ice for 2 min, following which 2 μL dNTP (2.5 mM each), 4 μL 5× Buffer, 0.5 μL RNase inhibitor and 200 U M-MLV were added to the above mixture and were incubated at 25 ℃ for 10 min, 42 ℃ for 50 min and 80 ℃ for 10 min to obtain 20 μL cDNA samples for subsequent experiments. Next, the relative mRNA levels of Chac1, Fth1 and Gpx4 were normalized to rat to β-actin expression. The following primers were synthesized by General Biol (Chuzhou, China): rat chac1 forward 5′-GTGCTTGGTGGCTACGAC-3′ and reverse 5′-TCCAGGTGCTCATCTTGTG-3′; rat Fth1 forward 5′-TGCCAAATACTTTCTCCA-3′ and reverse 5′-CCAGTCATCACGGTCAG-3′; rat Gpx4 forward 5′-AGTTCGGGAGGCAGGAG-3′ and reverse 5′-CCACGCAGCCGTTCTTA-3′; rat β-actin forward 5′-GGAGATTACTGCCCTGGCTCCTAGC-3′ and reverse 5′-GGCCGGACTCATCGTACTCCTGCTT-3′. The 20 μL reaction system consisted of 1 μL cDNA, 0.5 μL primers (10 μM), 0.3 μL SYBR Green (Solarbio, Beijing, China), 10 μL 2× Taq PCR MasterMix (Solarbio, Beijing, China) and ddH_2O. RT-qPCR was conducted with the following thermocycling conditions: 40 cycles of initial denaturation at 95 °C for 5 min, followed by denaturation at 95 °C for 10 s, annealing at 60 °C for 10 s, and extension at 72 °C for 15 s. Subsequently, there was an incubation step at 72 °C for 90 s, followed by a cooling step at 40 °C for 1 min. A melting curve analysis was conducted by ramping from 60 °C to 94 °C at 1 °C increments for 1 s each. Finally, the reaction was concluded with an incubation at 25 °C for 1–2 min.

2.5 Western blot

Total protein was isolated from the ileum tissue and IEC-6 cells using RIPA lysis buffer with 1% protease inhibitor (PR20032, Proteintech Group, Inc., Wuhan, China). Following the determination of protein concentration using a BCA kit (PK10026, Proteintech Group, Inc., Wuhan, China), the proteins were separated by sodium dodecyl sulfate - polyacrylamide gel electrophoresis (SDS-PAGE) and transferred into the polyvinylidene fluoride (PVDF) membrane (LC2005, Thermo Fisher Scientific, Pittsburgh, PA, USA). After incubation with 5% skim milk, the membranes were incubated with primary antibodies at 4 °C overnight. The primary antibodies included Chac1 antibody (dilution, 1:1000; cat. no. bs-6795R, Bioss), Gpx4 antibody (dilution, 1:1000; cat. no. A1933, ABclonal), Fth1 antibody (dilution, 1:1000; cat. no. DF6278, Affinity), and β-actin antibody (dilution, 1:20,000; cat. no. 66009-1-Ig, Proteintech). Subsequently, the washed membranes were incubated with HRP-labeled goat anti-rabbit IgG (dilution, 1:10,000; cat. no. SA00001-2, Proteintech) and HRP-labeled goat anti-mouse IgG (dilution, 1:10,000; cat. no. SA00001-1, Proteintech) for 40 min at 37 °C. The blots were then visualized using a hypersensitive ECL chemiluminescence detection kit (PK10003, Proteintech Group, Inc., Wuhan, China).

2.6 Immunofluorescence staining

Ileum tissue sections, embedded in paraffin, were incubated with primary antibodies, including anti-cytokeratin18 (CK18) (dilution, 1:200; cat. no. 66187-1-Ig, Proteintech) and anti-Chac1 (dilution, 1:200; cat. no. bs-6795R, Bioss), overnight at 4 °C. After rinsing with PBS, the sections were then treated with Cy3-labeled goat anti-rabbit IgG (dilution, 1:200; cat. no. SA00009-2, Proteintech) and FITC-labeled goat anti-mouse IgG (dilution, 1:200; cat. no. SA00003-1, Proteintech) for 90 min at room temperature. Subsequently, 4′,6-diamidino-2-phenylindole (DAPI) was used for nuclear staining, and images were captured at 400× magnification using an Olympus BX53 microscope (Tokyo, Japan). Furrhtermore additional sections were incubated with anti-occludin (dilution, 1:100; cat. no. DF7504, Affinity) and anti-zonula occludens-1 (ZO-1) (dilution, 1:100; cat. no. AF5145, Affinity) antibodies overnight at 4 °C, then subjected to incubation with Cy3-labeled goat anti-rabbit IgG (dilution, 1:200; cat. no. SA00009-2, Proteintech) for 60 min at room temperature. After DAPI staining of the nuclei, the cells were assessed using the Olympus BX53 microscope at 400× magnification.

2.7 Immunohistochemistry (IHC)

Ileum tissue sections were incubated with anti-Gpx4 (dilution, 1:100, cat. no. A1933, ABclonal) or anti-Fth1 (dilution, 1:100, cat. no. DF6278, Affinity) antibodies in the dark at 4 °C overnight. The samples were then incubated in HRP-labeled goat anti-rabbit IgG (dilution, 1:100; cat. no. SE134, Solarbio) for 45 min in the dark at room temperature. Following immersion in PBS, the sections were stained using the horseradish catalase DAB color kit (C520017, Sangon Biotech, Shanghai, China) at 37 °C for 10 min, and after staining with hematoxylin, the samples were assessed and captured under a BX53 microscope (Olympus, Tokyo, Japan).

2.8 Enzyme-linked immunosorbent assay (ELISA)

The concentration of I-FABP in the plasma was determined using a rat I-FABP ELISA kit (ER1068, Wuhan Fine Biotech, Wuhan, China) according to the manufacturer's protocols. Briefly, the samples were added into cultured wells and incubated at 37 °C for 90 min. After washing, 100 μL biotin-labeled antibody was added to the wells, followed by covering the membrane and incubation at 37 °C for 60 min. Subsequently, 100 μL of HRP-streptavidin (SABC) was added to each well and incubated at 37 °C for 30 min. After the 90 μL TMB substrate was added and incubated at 37 °C for 10–20 min in the dark, the reaction was stopped by 50 μL stop solution per well. The optical density (OD) value was estimated using a microplate reader (ELX-800, BioTek, Winooski, VT, USA) at 450 nm.

2.9 Lipid peroxidation (LPO), malondialdehyde (MDA), glutathione (GSH) and ferrous ion (Fe^{2+}) assays

After tissue homogenization, the samples were centrifuged at 2500 rpm for 10 min, and the supernatants were collected. Protein concentration was determined using a BCA kit (P0011, Beyotime Biotech, Shanghai, China). Then, the levels of LPO, MDA, GSH and Fe^{2+} in ileum tissues or IEC-6 cells were assessed using respective assay kits: LPO assay kit (A106, Jiancheng, Nanjing, China), MDA assay kit (A003-1, Jiancheng, Nanjing, China), reduced GSH assay kit (A006-2, Jiancheng, Nanjing, China), and ferrous iron colorimetric assay kit (E-BC-K881-M, Elabscience, Wuhan, China), following to the manufacturer's instructions.

2.10 Reactive oxygen species (ROS) assay

ROS production was assessed with dichlorofluorescein diacetate (DCFH-DA) and was examined using a ROS detection assay kit (S0033S, Beyotime Biotech, Shanghai, China). Ileum tissues were incubated with RIPA lysis, followed by centrifugation for 30 min. The supernatant was incubated with DCFH-DA in an incubator at 37 °C for 30 min. Subsequently, ROS was measured using a flow cytometer (NovoCyte, Agilent Technologies, Santa Clara, CA, USA). IEC-6 cells were incubated with DCFH-DA at 37 °C for 30 min, and the fluorescence was observed under an IX53 fluorescence microscopy (Olympus, Tokyo, Japan).

2.11 Cell counting kit 8 (CCK-8) assay

Cells (5×10^3 per well) were seeded in 96-well plates, and after transfection using shNC and shChac1 for 48 h, they were cultured under hypoxic conditions for 4 h, followed by recovery in a condition of normal oxygen content for 3 h. CCK-8 reagent (KGA317, KeyGen Biotech., Nanjing, China) was added into the cells and incubated in an incubator with 5% CO_2 at 37 °C for 2 h. Lastly, cell viability was analyzed at 450 nm using a microplate reader (800TS, BioTek, Winooski, VT, USA).

2.12 Statistical analysis

Data analysis was performed using GraphPad Prism software (version 7.0, San Diego, CA, USA), and the results are presented as means ± standard deviation (SD). The relative mRNA levels detected by RT-qPCR were normalized to β-actin expression. Statistical significance of differences between two groups was determined using unpaired Student's *t*-test, while differences among four groups were assessed using the ordinary one-way analysis of variance (ANOVA), followed by the Tukey's multiple comparisons test. Specifically, the difference of Chac1 mRNA expression in the ileum between the sham group and HS rat model was determined using unpaired Student's *t*-test. Subsequently, one-way ANOVA was used for the data from experiments (histopathological scoring, RT-qPCR, ELISA, ROS detection, examination of biochemical indicators and CCK-8 assay), followed by the Tukey's multiple comparisons test. A significance level of $p < 0.05$ was considered statistically significant.

3. Results

3.1 Chac1 is upregulated in the ileum of rats with hemorrhagic shock (HS)

The establishment of the rat model with HS was performed successfully. As shown in Fig. 1A, HS significantly increased the mRNA levels of Chac1 in the ileum tissue of the rat model. Furthermore, the protein expression of Chac1 was significantly elevated in the HS-induced rat model compared to the sham group (Fig. 1B). Immunofluorescence double-staining results confirmed the increased expression levels of both Chac1 and CK-18 in the ileum tissues of HS-induced rat model (Fig. 1C). These results indicate that HS could increase Chac1 expression in the at model's ileum tissues.

3.2 Knockdown of Chac1 alleviates the HS-induced injury of ileum tissue

Fig. 2A illustrates the pathological features of ileum tissues. H&E staining revealed that HS induced significant damage to the intestinal epithelial structure in the ileum tissue. Notably, the downregulation of Chac1 obviously reversed the expansion of the sub-epithelial space. Histological score further indicated that reduction of Chac1 significantly ameliorated the injury induced by HS in the ileum tissue of the rat model (Fig. 2B). Compared to the sham group, we observed a significant increase in the concentration of I-FABP in plasma obtained from the HS-induced rat model. However, following the injection of lentivirus carrying the shChac1, the I-FABP content was reduced in plasma of HS-reduced rat model (Fig. 2C). Previous studies have confirmed that the expression levels of occludin and ZO-1 are critical factors affecting the tight junction in the rat terminal ileum [26, 27]. immunofluorescence staining results indicated that HS decreased both occludin and ZO-1 expression levels in the ileum tissues and were significantly restored by depleting Chac1 (Fig. 2D,E). Thus, the downregulation of Chac1 attenuated the HS-induced impairment of the ileum tissue.

3.3 Reduction of Chac1 relieves the oxidative stress induced by HS in ileum tissue

ROS production labeled with DCFH-DA in ileum tissues was assessed *via* flow cytometry. As shown in Fig. 3A,B, HS significantly induced ROS production. However, when Chac1 was knocked down in the rat model, ROS levels were significantly. Furthermore, the LPO level was upregulated in the ileum tissues of HS-induced rat model, but this increase was significantly reduced by silencing Chac1 (Fig. 3C). Additionally, the concentration of GSH was decreased in the HS-induced rat model, while the reduction of Chac1 dramatically restored GSH content in the ileum tissues. Simultaneously, the absence of Chac1 reversed the upregulation of MDA concentration induced by HS in the ileum tissues (Fig. 3D). In summary, these results indicate that Chac1 plays a role in mitigating HS-induced oxidative stress in ileum tissue.

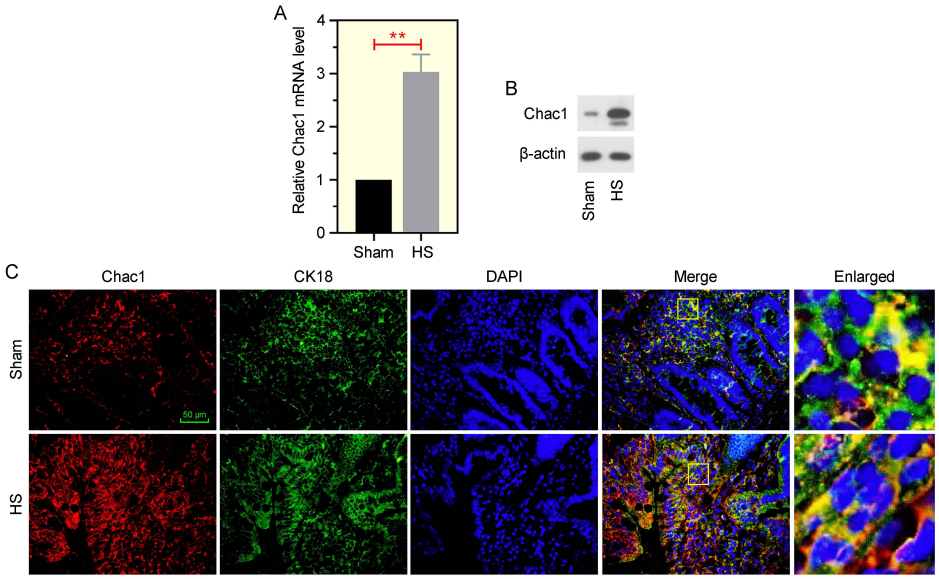

FIGURE 1. Chac1 is upregulated in the ileum of rats during HS. (A) Relative Chac1 mRNA expression assessed *via* RT-qPCR in ileum tissue. (B) Western blot analysis of Chac1 protein expression. (C) Double immunofluorescence staining for Chac1 and CK18 in ileum tissue from sham and HS rats. Scale bar: 50 μm. $^{**}p < 0.01$. HS: hemorrhagic shock; CK18: cytokeratin18; DAPI: 4′,6-diamidino-2-phenylindole.

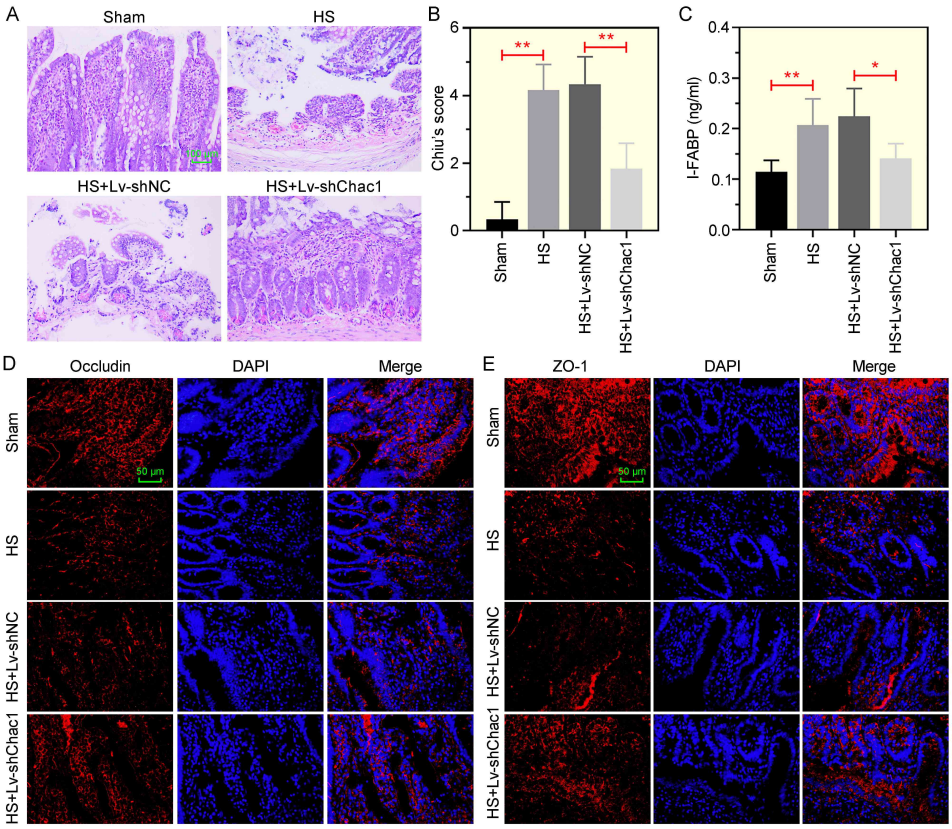

FIGURE 2. Chac1 knockdown alleviates the HS-induced injury of ileum tissues. (A) Representative H&E-stained images of ileum tissue from rats with different treatments assessing the impact of Chac1 on ileum damage. Scale bar: 100 μm. (B) Chiu's score for ileum tissue based on H&E staining. (C) Plasma I-FABP level measured by ELISA. (D,E) Immunofluorescence staining showing the expression of occludin and ZO-1 in ileum tissue. Scale bar: 50 μm. $^{*}p < 0.05$, $^{**}p < 0.01$. HS: hemorrhagic shock; Lv: lentivirus; shNC: negative control short hairpin RNA; I-FABP: intestinal fatty acid binding protein; ZO-1: zonula occludens-1; DAPI: 4′,6-diamidino-2-phenylindole.

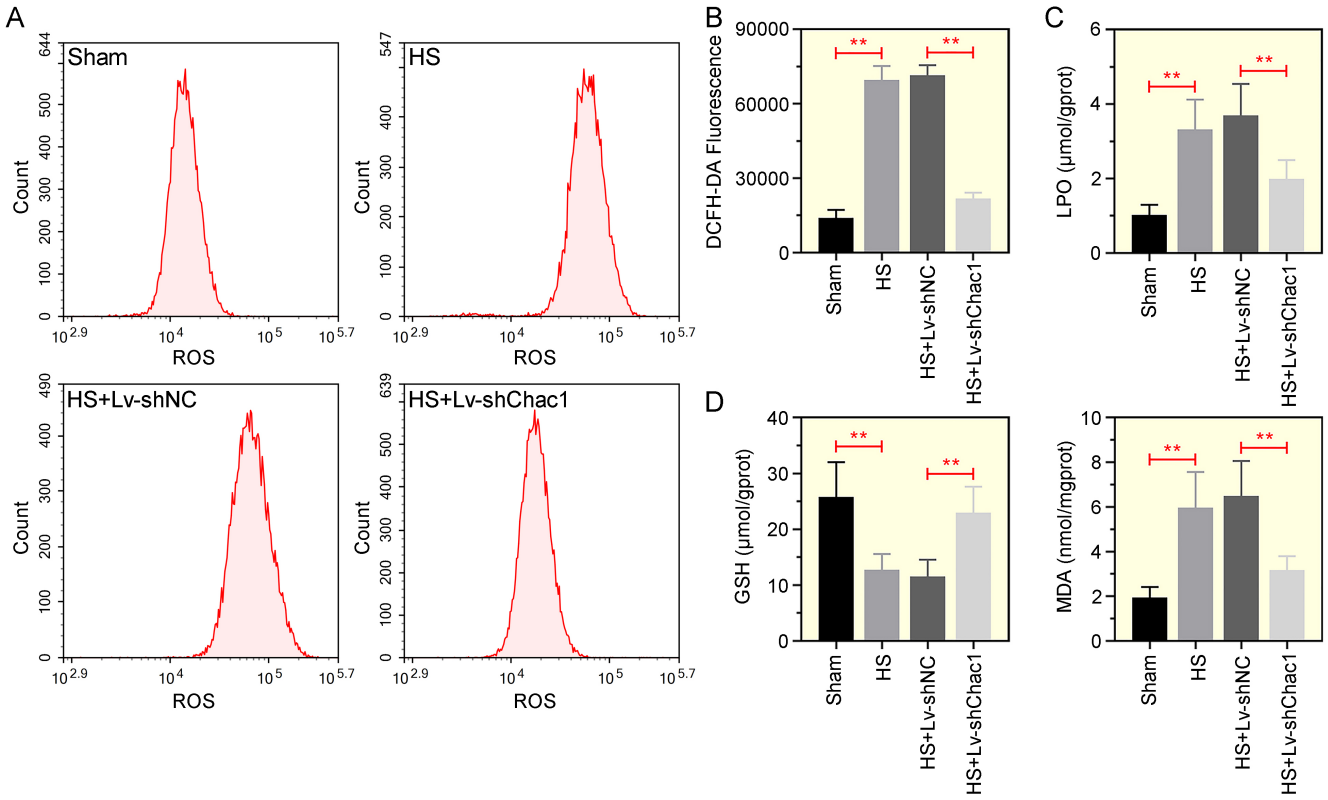

FIGURE 3. Chac1 reduction alleviates oxidative stress induced by HS in ileum tissues. (A) Flow cytometry detection of ROS production labeled with DCFH-DA. (B) Quantification of DCFH-DA fluorescence in ileum tissue. (C) Measurement of LPO levels in ileum tissues. (D) Assessment of GSH and MDA levels using respective kits. $^{**}p < 0.01$. DCFH-DA: dichlorofluorescein diacetate; LPO: Lipid peroxidation; MDA: malondialdehyde; GSH: glutathione.

3.4 Ferroptosis induced by HS is ameliorated by inhibiting Chac1 expression in ileum tissue

Previous studies have reported that Fth1 and Gpx4 are crucial proteins involved in ferroptosis [28, 29]. A decrease of Fth1 and Gpx4 levels is indicative of ferroptosis. The IHC results demonstrated that the protein expression of Fth1 and Gpx4 was significantly suppressed by HS treatment. However, following the injection of lentivirus-carried shChac1, the expression levels of Fth1 and Gpx4 in the ileum tissues were upregulated (Fig. 4A). Furthermore, the mRNA levels of Fth1 and Gpx4 declined by HS, which had declined due to HS, were significantly reversed by the depletion of Chac1 in the ileum tissues (Fig. 4B). Additionally, the concentration of Fe^{2+}, which had increased as a result of HS treatment, was reduced in the Chac1-silenced rat model with HS (Fig. 4C). Overall, these findings indicate that ferroptosis is induced by HS and can be alleviated by the downregulation of Chac1 expression in the ileum tissues of the rat model.

3.5 Silence of Chac1 attenuates the oxidative stress induced by hypoxia/reoxygenation (H/R) in IEC-6 cells

The mRNA expression level of Chac1 was found to be upregulated in H/R-induced IEC-6 cells. In addition, compared to H/R cells transfected with shNC, Chac1 expression was significantly decreased following the transfection of shChac1 (Fig. 5A). Likewise, Chac1 protein expression, induced by H/R, was significantly reduced by shChac1 in IEC-6 cells (Fig. 5B). Furthermore, after the H/R treatment, the GSH level was significantly suppressed, while the MDA was elevated in IEC-6 cells. However, the reduction of GSH and the increase of MDA induced by H/R were significantly reversed following the inhibition of Chac1 expression (Fig. 5C). ROS production, as labeled by DCFH-DA, was induced by H/R in IEC-6 cells. However, when the cells were transfected with shChac1, excessive ROS production was inhibited (Fig. 5D). Therefore, these results suggest that the oxidative stress induced by H/R could be impeded by the absence of Chac1 in IEC-6 cells.

3.6 Downregulation of Chac1 mitigates ferroptosis in H/R-induced IEC-6 cells

Fig. 6A illustrates that H/R treatment suppressed IEC-6 cell viability, but after the transfection of shChac1, the cell viability was significantly improved. Fig. 6B shows that the protein expressions of Gpx4 and Fth1 were reduced in the H/R-treated cells but significantly upregulated in IEC-6 cells when Chac1 was depleted. Moreover, the concentration of Fe^{2+} was significantly increased following H/R treatment, which could be effectively counteracted by suppressing Chac1 levels in IEC-6 cells (Fig. 6C). Overall, the absence of Chac1 effectively inhibited H/R-induced ferroptosis in IEC-6 cells.

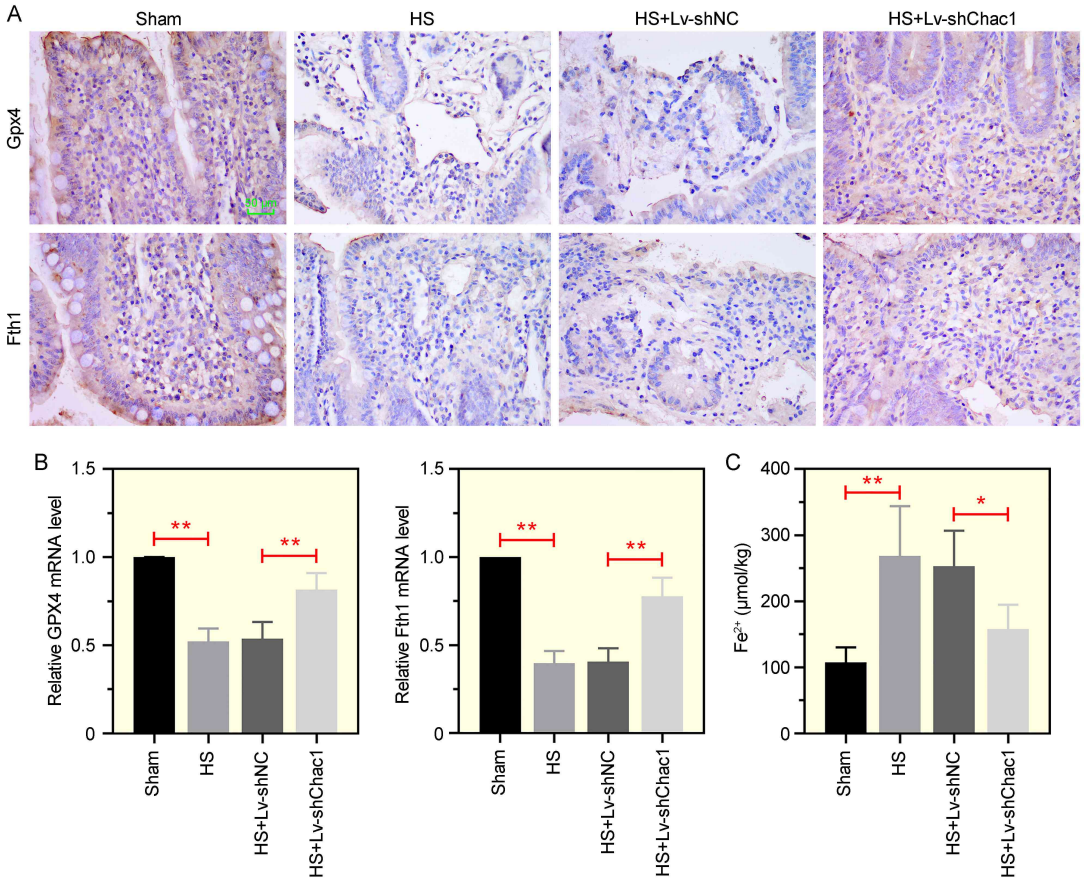

FIGURE 4. Ferroptosis induced by HS is ameliorated by inhibiting Chac1 expression in ileum tissues. (A) Immunohistochemistry staining to assess Gpx4 and Fth1 expression in ileum tissue. Scale bar: 50 μm. (B) Relative mRNA levels of Gpx4 and Fth1 determined by RT-qPCR. (C) Measurement of iron content in ileum tissue. *$p < 0.05$, **$p < 0.01$. Gpx4: glutathione peroxidase 4; Fth1: ferritin heavy chain.

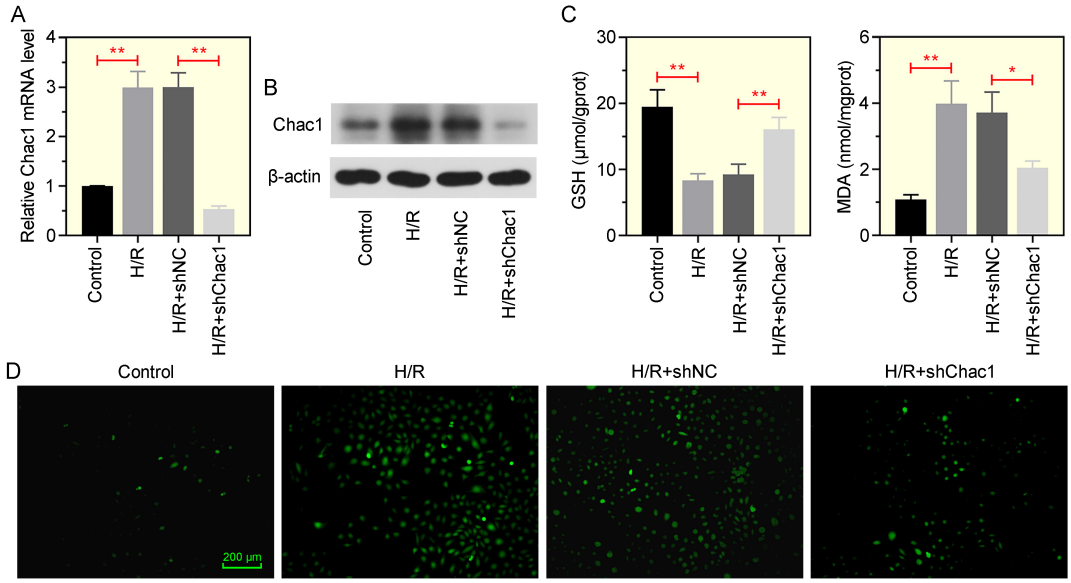

FIGURE 5. Silencing of Chac1 attenuates the oxidative stress induced by H/R in IEC-6 cells. (A,B) Relative mRNA and protein expression of Chac1 in H/R-treated IEC-6 cells. (C) Levels of GSH and MDA in IEC-6 cells. (D) Immunofluorescence staining showing ROS levels marked by DCFH-DA in IEC-6 cells. Scale bar: 200 μm. *$p < 0.05$, **$p < 0.01$. H/R: hypoxia/reoxygenation; IEC-6: rat small intestine crypt epithelial cells; MDA: malondialdehyde; GSH: glutathione; DCFH-DA: dichlorofluorescein diacetate; ROS: reactive oxygen species.

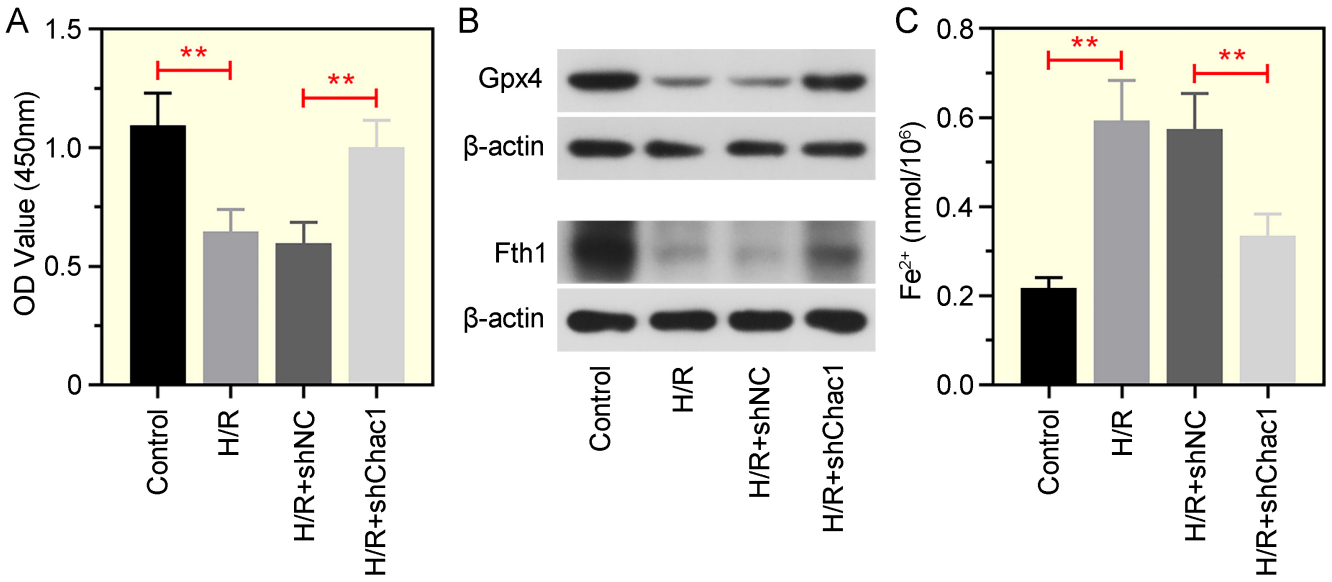

FIGURE 6. Chac1 downregulation mitigates ferroptosis in H/R-induced IEC-6 cells. (A) Cell viability assessed by CCK-8 assay. (B) Western blot analysis of Gpx4 and Fth1 protein expression. (C) Measurement of iron content in the respective groups. $^{**}p < 0.01$. Gpx4: glutathione peroxidase 4; Fth1: ferritin heavy chain.

4. Discussion

Severe blood loss results in systemic cellular anoxic stress, leading to the onset of HS [30], which is often accompanied by oxidative stress and ferroptosis [31, 32]. Importantly, damage to adherent junctions and tight junctions (TJ) is closely linked to intestinal barrier impairment and dysfunction [33]. Among these junctions, the transmembrane protein occludin and ZO-1 play vital roles in maintaining the normal structure and morphology of intestinal epithelial cells [34]. For instance, elevated levels of occludin and ZO-1 induced by dietary glucose oxidase have been shown to protect the integrity of intestinal barrier and maintain the microbiota balance in broilers ileum tissues [35]. Conversely, in an *in vitro* model of LPS-induced septicity-like intestinal injury, the expression levels of ZO-1 and occludin was reported to be decreased [36]. In addition, the expression of occludin and ZO-1 in intestinal tissues was reported to increase following the treatment of intestinal injury and dysfunction in septic mice, [37]. In line with these observations, our study identified a notable reduction in the expression levels of occludin and ZO-1 in HS-induced intestinal injury. Importantly, their expression levels were subsequently elevated in the absence of Chac1 in the HS rat model, signifying that HS instigates damage to intestinal epithelial structure, while the downregulation of Chac1 expression ameliorates this injury, which were confirmed by H&E staining. Overall, this study presents a promising strategy for alleviating HS-induced intestinal damage.

Oxidative stress and ferroptosis have been identified as vital processes in HS induced-injury. Patients with traumatic hemorrhagic shock often experience oxidative stress, as evidenced by the downregulation of MDA, indicating an improvement in oxidative stress [38]. Ferroptosis, a form of regulated cell death, is dependent on iron concentration and ROS accumulation [39] and has been implicated in various pathological conditions, including traumatic hemorrhagic shock [40]. Moreover, specific inhibitors targeting ferroptosis have shown promise in alleviating intestinal injury induced by HS [41]. In this study, DCFH-DA labeling revealed an increase in ROS production in the ileum tissue of HS rat models. HS led to elevated levels of LPO and MDA, coupled with a reduction in GSH concentration in the ileum tissue. Additionally, HS suppressed the expression of Gpx4 and Fth1 while significantly increasing the concentration of Fe^{2+} in the ileum tissue of HS rat models. These findings provided further evidence that HS induces oxidative stress and ferroptosis in the ileum tissue of rat models. Likewise, ROS production was elevated in H/R-treated IEC-6 cells, accompanied by reduced GSH levels and increased MDA. Cell viability was notably decreased in H/R-treated cells compared to the control group. Furthermore, H/R treatment resulted in decreased protein expression of Gpx4 and Fth1, along with increased Fe^{2+} concentration. Thus, it could be deduced that HS-induced intestinal injury is mediated by oxidative stress and ferroptosis in the ileum tissue and intestinal epithelial cells. Chac1, identified as an effective antioxidant, can suppress oxidative stress and ferroptosis, and our results suggest that it could be a potential therapeutic target for alleviating intestinal damage.

Consistent with our prior sequencing data, Chac1 exhibited a significant upregulation in the ileum tissue of HS rat model. Subsequently, RT-qPCR, western blot and immunofluorescence staining assays confirmed that HS induced an increase in both mRNA and protein levels of Chac1 in ileum tissue. Chac1 has been previously linked to GSH degradation and shown to impact inflammatory responses and apoptosis in lung epithelial cells [42]. Notably, Chac1 knockdown has been shown to mitigate the decrease in GSH levels and apoptosis induced by heat exposure in porcine intestinal epithelial cells [43]. Our results further elucidated the role of Chac1 in HS-induced intestinal injury. Knockdown of Chac1 ameliorated

intestinal structure damaged caused by HS and upregulated the expression of occluding and ZO-1, thereby reducing TJ permeability in the rat terminal ileum. Moreover, Chac1 downregulation mitigated oxidative stress induced by HS by decreasing the ROS production and reducing the levels of LPO and MDA, while elevating GSH levels in the ileum tissues. The increase in Gpx4 and Fth1 expression and the decrease in Fe^{2+} concentration following Chac1 silencing confirmed the suppression of ferroptosis associated with HS-induced intestinal injury in ileum tissues. In the H/R-treated IEC-6 cells, Chac1 knockdown increased GSH levels, reduced MDA levels, and suppressed ROS production, indicating the attenuation of oxidative stress induced by H/R. Furthermore, cell viability improved after shChac1 transfection in H/R-treated cells. The observed upregulation of Gpx4 and Fth1expression and the reduction in Fe^{2+} concentration in Chac1-reduced IEC-6 cells further supported that our results point to the amelioration of HS-triggered intestinal injury through Chac1-mediated suppression of oxidative stress and ferroptosis, both *in vitro* and *in vivo*.

This present study shed light on the role of Chac1 in intestinal injury induced by HS using a rat model. Our findings suggest that Chac1 could be a promising target for mitigating such injuries. However, there are certain limitations that should be addressed. While our results showed the potential significance of Chac1 in this context, the specific signaling pathways or downstream factors involved in its protective effect remain unclear. Thus, additional research is required to fill this knowledge gap.

5. Conclusions

In summary, this present study suggests that Chac1 is a key regulator of oxidative stress and ferroptosis, and acts as a protective factor against intestinal injury and dysfunction induced by HS. To our knowledge, this is the first study to elucidate the protective role of Chac1, which operates through the modulation of occludin, ZO-1, Gpx4, Fth1, LPO, GSH, MDA and Fe^{2+} levels. Taken together, these findings offer a promising avenue for mitigating HS-induced intestinal injury.

AVAILABILITY OF DATA AND MATERIALS

The data presented in this study are available on reasonable request from the corresponding author.

AUTHOR CONTRIBUTIONS

XG and JDZ—designed the research study. HY and YW—performed the research. WMZ and CX—analyzed the data. HY and YW—wrote the manuscript. All authors read and approved the final manuscript.

ETHICS APPROVAL AND CONSENT TO PARTICIPATE

All animal experiments adhered to the guidelines outlined in the National Institutes of Health Animal Use and Care Guidelines and were approved by the Medical Ethics Committee of Wuxi 9th People's Hospital Affiliated to Soochow University (Approval No. KT2021026).

ACKNOWLEDGMENT

Not applicable.

FUNDING

This work was supported by the Project of Wuxi Science and Technology Association (grant No. KX-23-B030), the Major Scientific Projects of Wuxi Municipal Healthy Commission (grant No. Z202105) and the Wuxi Top Medical Expert Team of "Taihu Talent Program".

CONFLICT OF INTEREST

The authors declare no conflict of interest.

REFERENCES

[1] Cannon JW. Hemorrhagic Shock. New England Journal of Medicine. 2018; 378: 370–379.

[2] Manson J, Hoffman R, Chen S, Ramadan MH, Billiar TR. Innate-like lymphocytes are immediate participants in the hyper-acute immune response to trauma and hemorrhagic shock. Frontiers in Immunology. 2019; 10: 1501.

[3] Niu Q, Du F, Yang X, Yang X, Wang X. Carbon monoxide-releasing molecule 2 inhibits inflammation associated with intestinal ischemia-reperfusion injury in a rat model of hemorrhagic shock. International Immunopharmacology. 2022; 113: 109441.

[4] Saracoglu A, Saracoglu K, Ergun I, Yildirim M, Akca M, Demirtas C, *et al*. The effects of hydroxyethyl starch and gelatine on lung tissue and coagulation during the resuscitation of rats with traumatic haemorrhagic shock. Anaesthesiology intensive therapy. 2022; 54: 393–401.

[5] Grosheva I, Zheng D, Levy M, Polansky O, Lichtenstein A, Golani O, *et al*. High-throughput screen identifies host and microbiota regulators of intestinal barrier function. Gastroenterology. 2020; 159: 1807–1823.

[6] Zhang L, Xin Y, Song R, Zheng W, Hu J, Wang J, *et al*. CORM-3 alleviates the intestinal injury in a rodent model of hemorrhage shock and resuscitation: roles of GFAP-positive glia. Journal of Molecular Histology. 2023; 54: 271–282.

[7] Canovai E, Farré R, Accarie A, Lauriola M, De Hertogh G, Vanuytsel T, *et al*. INT-767-A dual farnesoid-X receptor (FXR) and Takeda G protein-coupled receptor-5 (TGR5) agonist improves survival in rats and attenuates intestinal ischemia reperfusion injury. International Journal of Molecular Sciences. 2023; 24: 14881.

[8] Garcia-Alonso I, Velasco-Oraa X, Cearra I, Iturrizaga Correcher S, Mar Medina C, Alonso-Varona A, *et al*. Prophylactic treatment of intestinal ischemia-reperfusion injury reduces mucosal damage and improves intestinal absorption. Journal of Inflammation Research. 2023; 16: 4141–4152.

[9] Munley JA, Kelly LS, Park G, Gillies GS, Pons EE, Kannan KB, *et al*. Multicompartmental traumatic injury induces sex-specific alterations in the gut microbiome. Journal of Trauma and Acute Care Surgery. 2023; 95: 30–38.

[10] Li Y, Cao Y, Xiao J, Shang J, Tan Q, Ping F, *et al*. Inhibitor of apoptosis-stimulating protein of p53 inhibits ferroptosis and alleviates intestinal ischemia/reperfusion-induced acute lung injury. Cell Death & Differentiation. 2020; 27: 2635–2650.

[11] Deng F, Zhao BC, Yang X, Lin ZB, Sun QS, Wang YF, *et al*. The gut microbiota metabolite capsiate promotes Gpx4 expression by activating *TRPV1* to inhibit intestinal ischemia reperfusion-induced ferroptosis. Gut Microbes. 2021; 13 :1–21.

[12] Masior Ł, Grąt M. Methods of attenuating ischemia-reperfusion injury in liver transplantation for hepatocellular carcinoma. International Journal of Molecular Sciences. 2021; 22: 8229.
[13] Mehta V, Suman P, Chander H. High levels of unfolded protein response component CHAC1 associates with cancer progression signatures in malignant breast cancer tissues. Clinical & Translational Oncology. 2022; 24: 2351–2365.
[14] Yang M, Chen Y, Huang X, Shen F, Meng Y. ETS1 ameliorates hyperoxia-induced bronchopulmonary dysplasia in mice by activating Nrf2/HO-1 mediated ferroptosis. Lung. 2023; 201: 425–441.
[15] Kim M, Lee Y, Lee M. Hypoxia-specific anti-RAGE exosomes for nose-to-brain delivery of anti-miR-181a oligonucleotide in an ischemic stroke model. Nanoscale. 2021; 13: 14166–14178.
[16] Li XN, Shang NY, Kang YY, Sheng N, Lan JQ, Tang JS, *et al*. Caffeic acid alleviates cerebral ischemic injury in rats by resisting ferroptosis *via* Nrf2 signaling pathway. To be published in Acta pharmacologica Sinica. 2023. [Preprint].
[17] Zhang J, Bi J, Ren Y, Du Z, Li T, Wang T, *et al*. Involvement of GPX4 in irisin's protection against ischemia reperfusion-induced acute kidney injury. Journal of Cellular Physiology. 2021; 236: 931–945.
[18] Gou Z, Su X, Hu X, Zhou Y, Huang L, Fan Y, *et al*. Melatonin improves hypoxic-ischemic brain damage through the Akt/Nrf2/Gpx4 signaling pathway. Brain Research Bulletin. 2020; 163: 40–48.
[19] Xu J, Zhao L, Zhang X, Ying K, Zhou R, Cai W, *et al*. Salidroside ameliorates acetaminophen-induced acute liver injury through the inhibition of endoplasmic reticulum stress-mediated ferroptosis by activating the AMPK/SIRT1 pathway. Ecotoxicology and Environmental Safety. 2023; 262: 115331.
[20] Stockwell BR, Jiang X, Gu W. Emerging mechanisms and disease relevance of ferroptosis. Trends in Cell Biology. 2020; 30: 478–490.
[21] Zhou Z, Zhang H. CHAC1 exacerbates LPS-induced ferroptosis and apoptosis in HK-2 cells by promoting oxidative stress. Allergologia et Immunopathologia. 2023; 51: 99–110.
[22] Liu Y, Wu D, Fu Q, Hao S, Gu Y, Zhao W, *et al*. CHAC1 as a Novel contributor of ferroptosis in retinal pigment epithelial cells with oxidative damage. International Journal of Molecular Sciences. 2023; 24: 1582.
[23] Li D, Liu S, Xu J, Chen L, Xu C, Chen F, *et al*. Ferroptosis-related gene CHAC1 is a valid indicator for the poor prognosis of kidney renal clear cell carcinoma. Journal of Cellular and Molecular Medicine. 2021; 25: 3610–3621.
[24] Shi HP, Deitch EA, Xu DZ, Lu Q, Hauser CJ. Hypertonic saline improves intestinal mucosa barrier function and lung injury after trauma-hemorrhagic shock. Shock. 2002; 17: 496–501.
[25] Chiu C. Intestinal mucosal lesion in low-flow states. Archives of Surgery. 1970; 101: 478.
[26] Chen F, Ohashi N, Li W, Eckman C, Nguyen JH. Disruptions of occludin and claudin-5 in brain endothelial cells *in vitro* and in brains of mice with acute liver failure. Hepatology. 2009; 50: 1914–1923.
[27] Mazzon E, Crisafulli C, Galuppo M, Cuzzocrea S. Role of peroxisome proliferator-activated receptor-alpha in ileum tight junction alteration in mouse model of restraint stress. American Journal of Physiology Gastrointestinal and Liver Physiology. 2009; 297: G488–505.
[28] Xie Y, Hou W, Song X, Yu Y, Huang J, Sun X, *et al*. Ferroptosis: process and function. Cell Death & Differentiation. 2016; 23: 369–379.
[29] Cao JY, Dixon SJ. Mechanisms of ferroptosis. Cellular and Molecular Life Sciences. 2016; 73: 2195–2209.
[30] Yadav VR, Hussain A, Sahoo K, Awasthi V. Remediation of hemorrhagic shock-induced intestinal barrier dysfunction by treatment with diphenyldihaloketones EF24 and CLEFMA. Journal of Pharmacology and Experimental Therapeutics. 2014; 351: 413–422.
[31] Gao M, Monian P, Quadri N, Ramasamy R, Jiang X. Glutaminolysis and transferrin regulate ferroptosis. Molecular Cell. 2015; 59: 298–308.
[32] Yao Z, Liu N, Lin H, Zhou Y. Proanthocyanidin alleviates liver ischemia/reperfusion injury by suppressing autophagy and apoptosis *via* the PPARα/PGC1α signaling pathway. Journal of Clinical and Translational Hepatology. 2023; 11: 1329–1340.
[33] Groschwitz KR, Hogan SP. Intestinal barrier function: molecular regulation and disease pathogenesis. Journal of Allergy and Clinical Immunology. 2009; 124: 3–20.
[34] Hartsock A, Nelson WJ. Adherens and tight junctions: structure, function and connections to the actin cytoskeleton. Biochimica Et Biophysica Acta—Biomembranes. 2008; 1778: 660–669.
[35] Zhao Y, Fu J, Li P, Chen N, Liu Y, Liu D, *et al*. Effects of dietary glucose oxidase on growth performance and intestinal health of AA broilers challenged by Clostridium perfringens. Poultry Science. 2022; 101: 101553.
[36] Huang S, Zhang S, Chen L, Pan X, Wen Z, Chen Y, *et al*. Lipopolysaccharide induced intestinal epithelial injury: a novel organoids-based model for sepsis *in vitro*. Chinese Medical Journal. 2022; 135: 2232–2239.
[37] Deng J, Huang SQ, Liu JT, Li W, Zeng JR, Shi HQ, *et al*. Protective effect of mesenchymal stem cell transplantation on intestinal injury in septic mice and its mechanism. Journal of Sichuan University Medical. 2023; 54: 565–573. (In Chinese)
[38] Luo D, Pan Q, Wang L, Zhao W, Bao W. Effects of alprostadil combined with edaravone on inflammation, oxidative stress and pulmonary function in patients with traumatic hemorrhagic shock. Cellular and Molecular Biology. 2022; 68: 123–128.
[39] Dixon S, Lemberg K, Lamprecht M, Skouta R, Zaitsev E, Gleason C, *et al*. Ferroptosis: an iron-dependent form of nonapoptotic cell death. Cell. 2012; 149: 1060–1072.
[40] Angeli JPF, Shah R, Pratt DA, Conrad M. Ferroptosis inhibition: mechanisms and opportunities. Trends in Pharmacological Sciences. 2017; 38: 489–498.
[41] Tuo Q, Lei P, Jackman KA, Li X, Xiong H, Li X, *et al*. Tau-mediated iron export prevents ferroptotic damage after ischemic stroke. Molecular Psychiatry. 2017; 22: 1520–1530.
[42] Perra L, Balloy V, Foussignière T, Moissenet D, Petat H, Mungrue IN, *et al*. CHAC1 is differentially expressed in normal and cystic fibrosis bronchial epithelial cells and regulates the inflammatory response induced by pseudomonas aeruginosa. Frontiers in Immunology. 2018; 9: 2823.
[43] Cui Y, Zhou X, Chen L, Tang Z, Mo F, Li XC, *et al*. Crosstalk between endoplasmic reticulum stress and oxidative stress in heat exposure-induced apoptosis is dependent on the ATF4–CHOP–CHAC1 signal pathway in IPEC-J2 cells. Journal of Agricultural and Food Chemistry. 2021; 69: 15495–15511.

How to cite this article: Hao Yao, Yan Wang, Wuming Zhou, Ce Xu, Xin Ge, Jiandong Zhu. Chac1 silencing mitigates hemorrhagic shock-induced intestinal injury by inhibiting oxidative stress and ferroptosis. Signa Vitae. 2023; 19(6): 184-193. doi: 10.22514/sv.2023.113.